AGU PUBLICATIONS

Global Biogeochemical Cycles

Supporting Information for

Update on the Temperature Corrections of Global Air-Sea CO_2 Flux Estimates

Yuanxu Dong[1,2], Dorothee C. E. Bakker[1]*, Thomas G. Bell[2], Boyin Huang[3], Peter Landschützer[4], Peter S. Liss[1], Mingxi Yang[2]

[1]Centre for Ocean and Atmospheric Sciences, School of Environmental Sciences, University of East Anglia, Norwich, UK; [2]Plymouth Marine Laboratory, Prospect Place, Plymouth, UK; [3]National Centers for Environmental Information, National Oceanic and Atmospheric Administration, Asheville, NC, USA; [4]Max Planck Institute for Meteorology, Hamburg, Germany

Correspondence to: Yuanxu Dong (Yuanxu.Dong@uea.ac.uk) and Dorothee C. E. Bakker (D.Bakker@uea.ac.uk)

Contents of this file

Additional Supporting Information (Files uploaded separately)

Dataset S1

Text S1. Conversion of CO_2 Concentration

The mole fraction of the equilibrated CO_2 (χCO_{2w}) in the equilibrator is measured by a gas analyzer and is then converted into CO_2 partial pressure (pCO_{2w_equ}) using the equilibrator temperature (T_{equ}, K) and pressure (P_{equ}, atm):

$$pCO_{2w\_equ} = \chi CO_{2w}(P_{equ} - pH_2O) \tag{S1}$$

where pH_2O (atm) is the water vapor pressure and can be calculated from T_{equ} and the seawater salinity (Pierrot et al., 2009). The pCO_{2w_equ} is then converted into fCO_{2w_equ} to correct for non-ideal behavior of the gas (Weiss, 1974):

$$fCO_{2w\_equ} = \gamma\, pCO_{2w\_equ} \tag{S2}$$

where the fugacity coefficient γ is ~0.996 (Bakker et al., 2014).

Text S2. The Timescale of Chemical Repartitioning and Water Mass Transport

The seawater carbonate system creates unique properties for air-sea CO_2 exchange. The seawater carbonate system includes several different carbonate species, i.e., CO_2, carbonic acid, bicarbonate, carbonate. Among these species, only CO_2 is directly involved in the air-sea CO_2 exchange. There is a dynamic equilibrium between these carbonate species. When the seawater temperature varies, these carbonate species repartition and gradually approach a new equilibrium. The relaxation time (the time after which a perturbation has reached e^{-1} of its initial value) for this equilibration depends on pH and temperature. For typical seawater (pH ~8.2, total dissolved inorganic carbon ~2000 μmol kg^{-1}, and salinity ~35) at ~25℃, the relaxation time is ~13 s (Johnson, 1982; Zeebe & Wolf-Gladrow, 2001). For warmer seawater (e.g., ~30℃), the relaxation time is shorter (~11 s) (Johnson, 1982; Zeebe & Wolf-Gladrow, 2001), while for colder seawater, the relaxation time is longer. Therefore, the timescale of the chemical repartitioning of the CO_2 system is at least 10 s. i.e., if the seawater temperature varies, more than 10 s is required for the carbonate species to approach equilibrium.

There is a temperature gradient in the thermal boundary layer (TBL), and the temperature at the top of the TBL is lower than that at the bottom of the TBL due to the cool skin effect. The typical thickness of the TBL (L) is 1 mm (Jähne, 2009). The mass boundary layer (MBL) is at the top of the TBL with a typical thickness of 0.1 mm (Jähne, 2009). Molecular diffusion dominates water mass transport within MBL. There is a viscous boundary layer (VBL) below the MBL and the VBL has a similar thickness as the TBL (i.e., L ~1 mm) (Jähne, 2009). Viscous dissipation dominates water mass transport in the VBL (Jähne, 2009). The kinematic viscosity (v) is ~1 mm^2 s^{-1} at 25℃ seawater (v is larger at colder seawater). So, the timescale of water mixing in the TBL (below the MBL) is ~1 s (L^2 / v).

Text S3. SST Dataset for Air-Sea CO_2 Flux Estimates

The SST data used for flux estimates differ between studies. Table S1 lists SST datasets used in eight global observation-based (i.e., fCO_2-based) air-sea CO_2 flux estimates. Within a specific study, the same global gap-free SST dataset is typically used for the calculation of Schmidt number, Sc, solubility at the base of the MBL, α_w, and at the air-sea interface, α_i, CO_2 fugacity in the atmosphere, fCO_{2a}, and for the fCO_{2w} mapping, while the *in-situ* bulk water temperature (T_{Bulk}) measured concurrently with fCO_{2w} is used for correcting individual fCO_{2w} from the equilibrator temperature to the seawater temperature.

An exception to the above is Watson et al. (2020), which co-located the DOISST v2.0 (1° × 1°, monthly data) (Reynolds et al., 2007) to the individual fCO_{2w} measurements in SOCAT (Goddijn-Murphy et al., 2015). The co-located DOISST v2.0 was used to re-calculate fCO_{2w} (via Equation 2 in the main text). Watson et al. (2020) showed that SOCAT SST is on average 0.13 ± 0.78 K higher than the co-located DOISST v2.0, and the SOCAT fCO_{2w} is on average 1.65 ± 11.98 µatm higher than the re-calculated fCO_{2w}. Watson et al. (2020) and this study are the only two studies that considered the cool skin effect. Watson et al. (2020) applied a constant cool skin correction (0.17 K) to the satellite subskin SST product (i.e., DOISST v2.0 minus 0.17 K) for the calculation of α_i and fCO_{2a}. In addition, Watson et al. (2020) used HadISST for the mapping process instead of the SST product used to calculate the other variables (i.e., DOISST v2.0).

As discussed in the main text, a global gap-free $T_{Subskin}$ product is an important practical SST for the air-sea CO_2 flux calculation. However, only some of the global gap-free SST products in Table S1 (MOISST v2, DOISST v2.0, OAFlux, and CCI SST v2.1) represent the subskin temperature, while the others (ASMD, ARMOR3D, MGDSST, HadISST) correspond to the temperature of bulk seawater.

Text S4. Comparison of Three Satellite SST Products

The satellite SST product is expected to provide a consistent subskin temperature which can be used for calculating global *Sc*, α_w, α_i, and fCO_{2a}, and for mapping fCO_{2w}. Recent research compared eight global gap-free satellite/blend SST products (ESA CCI SST v2.0, ERA5, HadISST1, DOISST v2.1, MUR25 v4.2, MGDSST, BoM Monthly SST, OSITASST) and showed that the global mean of these eight SST products ranges from 20.02 °C to 20.17 °C (for the period 2003-2018 with 95% confidence level) (Yang et al., 2021). So, a bias potentially exists in some or all of these satellite SST products. In addition, among these eight satellite SST products, only the CCI SST (Merchant et al., 2019; Merchant & Embury, 2020) and the DOISST (Huang et al., 2021; Reynolds et al., 2007) represent the subskin temperature (Yang et al., 2021). The other SST products provide a bulk temperature for a depth below the subskin. So, hereafter, only the CCI SST and the OISST (DOISST and MOISST) are assessed.

There are two types of OISST products: 1) 1° × 1°, monthly OI.V2 SST (MOISST), which is derived by linear interpolation of the 1° × 1°, weekly OI.v2 SST fields to daily fields which are then averaged over a month (Reynolds et al., 2002); 2) 1/4° × 1/4°, daily OISST v2 (Reynolds et al., 2007) which has been replaced by DOISST v2.1 (Huang et al., 2021) with some quality improvements for data from January 1, 2016, onwards. DOISST data are constructed differently than the MOISST, although both use satellite-derived SST data with a calibration based on *in-situ* measurements (including both ICOADS ship and drifting buoy SST) (Freeman et al., 2017; Xu & Ignatov, 2014). With the warm bias in the ICOADS ship SST well-recognized by the SST community (Huang et al., 2017; Kennedy et al., 2011, 2019), a constant (0.14 K) is subtracted from the ICOADS ship SST to compensate for the large scale (global mean) ship-buoy SST difference (Reynolds & Chelton, 2010) before it is used to calibrate the DOISST v2.0. In addition, the latest research shows that the bias in the ICOADS ship SST has substantially reduced since 2006 (Kennedy et al., 2019). So for the DOISST v2.1 dataset, the ship-buoy SST difference has been set to 0.14 K from 1981 to 2015 and to 0.01 K from 2016 onwards (Huang et al., 2021). However, the warm bias in the ICOADS ship SST is not corrected for when it is used for the calibration of the MOISST. So the DOISST tends to be lower than the monthly MOISST, particularly in the 1980s and 1990s when ship SST data were dominant (Banzon et al., 2016).

Here we test the agreement between the gridded drifting buoy SST (as a reference SST; Xu & Ignatov, 2014) and three satellite SST products: CCI SST v2.1, MOISST v2, DOISST v2.1. Figure S1a shows a comparison between different SST products. The DOISST v2.1 is on average 0.09 K lower than the buoy SST (red curve), while the MOISST v2 is on average 0.01 K lower than the buoy SST (blue curve). The orange curve shows that the CCI SST v2.1 is on average 0.05 K lower than the buoy SST.

Although MOISST v2 has the smallest bias, it is an old SST product and has not been updated for a long time. The standard deviation (SD) of MOISST minus the buoy SST (blue line in Figure S1b) is larger than that of DOISST v2.1 (or CCI SST v2.1) minus buoy SST (red and orange lines in Figure S1b). Therefore, we suggest that the MOISST should better not be used for air-sea CO_2 flux estimates.

The SD of DOISST v2.1 minus the buoy SST is similar to the SD of CCI SST v2.1 minus the buoy SST (red and orange line in Figure S1b). Therefore, both DOISST v2.1 and CCI SST v2.1 can be used for the air-sea CO_2 flux estimates (i.e., calculating global Sc, α_w, α_i, $f\mathrm{CO}_{2a}$, and mapping $f\mathrm{CO}_{2w}$). However, as the *in-situ* SST measurements were employed for the validation process, DOISST and MOISST are not fully independent from the *in-situ* SSTs. The CCI SST is independent from the *in-situ* SST dataset because the CCI SST is not calibrated against *in-situ* SST measurements as a reduced-state-vector optimal estimation algorithm (Merchant et al., 2019) is used instead.

The purple line in Figure S1b shows that the SD of CCI SST v2.1 minus DOISST v2.1 is ~0.5 K and decreasing to ~0.4 K in recent years, which suggests that there is a discrepancy between these two satellite SST products. the SD of DOISST v2.0 minus SOCAT SST is ~0.8 K. The large SDs suggest that using any co-located satellite SST products to calculate $f\mathrm{CO}_{2w}$ could significantly increase the uncertainty in $f\mathrm{CO}_{2w}$ and thus the uncertainty in the estimated air-sea CO_2 flux.

Text S5. Under-Sampling and inter-Annual Variation of the Bias Correction

Due to the limited measurements in SOCAT and buoy SST datasets, especially during the 1980s, many grid cells only have a small number of SOCAT and buoy SST measurements. The number of measurements in grid cells might influence the comparison between the SOCAT SST and the buoy SST. Figure S2a shows the under-sampling issue and its influence on the average of SOCAT SST minus buoy SST. If we consider all matched grid cells, the average of SOCAT SST minus buoy SST is ~0.02 K. But if we consider cells with at least 10 measurements, the average of SOCAT SST minus buoy SST is ~0.03 K. However, Figure S2b suggests that under-sampling does not significantly influence the latitudinal variation of SOCAT SST minus buoy SST.

Figure S3 shows the inter-annual variation of the number of cells with SOCAT measurements and the bias correction for the SOCAT SST. We apply the latitudinal-varying bias correction (red curve in Figure S2b) to account for the bias in the SOCAT SST (use buoy SST as the reference). However, as the number of SOCAT measurements varies with year, and the measurements in years before 1990 are limited (blue bars in Figure S3), we do not consider inter-annual variation of the latitudinal-varying bias correction. Thus, the same bias correction value is applied to a specific latitude for every year (every month) between 1982 and 2020. However, as the spatial distribution of the SOCAT measurements is different in different years, the annual mean bias correction varies with year (red line in Figure S3).

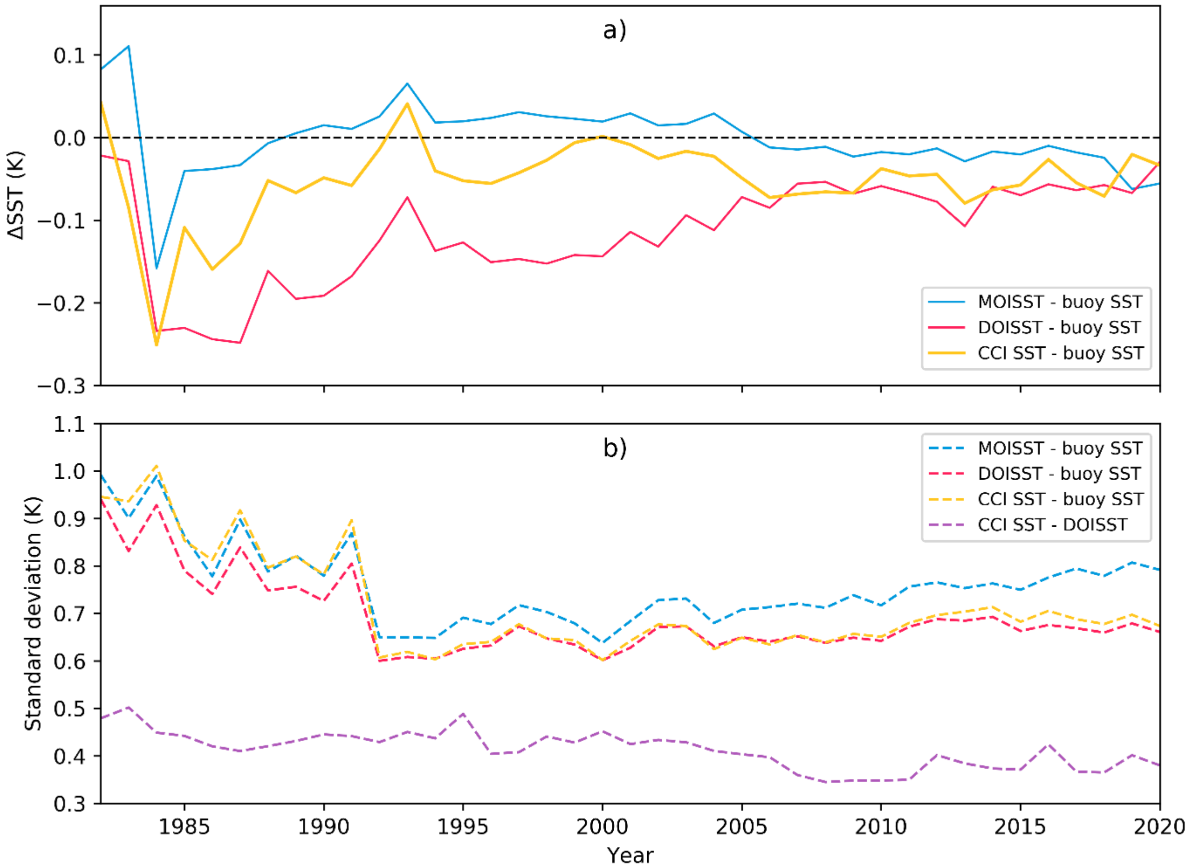

Figure S1. Time series of the global annual mean SST difference and its standard deviation between SST products. (a) The blue, red and orange lines represent the MOISST v2 (MOISST) minus drifting buoy SST, DOISST v2.1 (DOISST) minus buoy SST, and ESA CCI SST v2.1 (CCI SST) minus buoy SST, respectively. (b) The blue, red, orange, and purple dashed lines correspond to the standard deviation of MOISST minus buoy SST, DOISST minus buoy SST, CCI SST and buoy SST, and CCI SST minus DOISST, respectively.

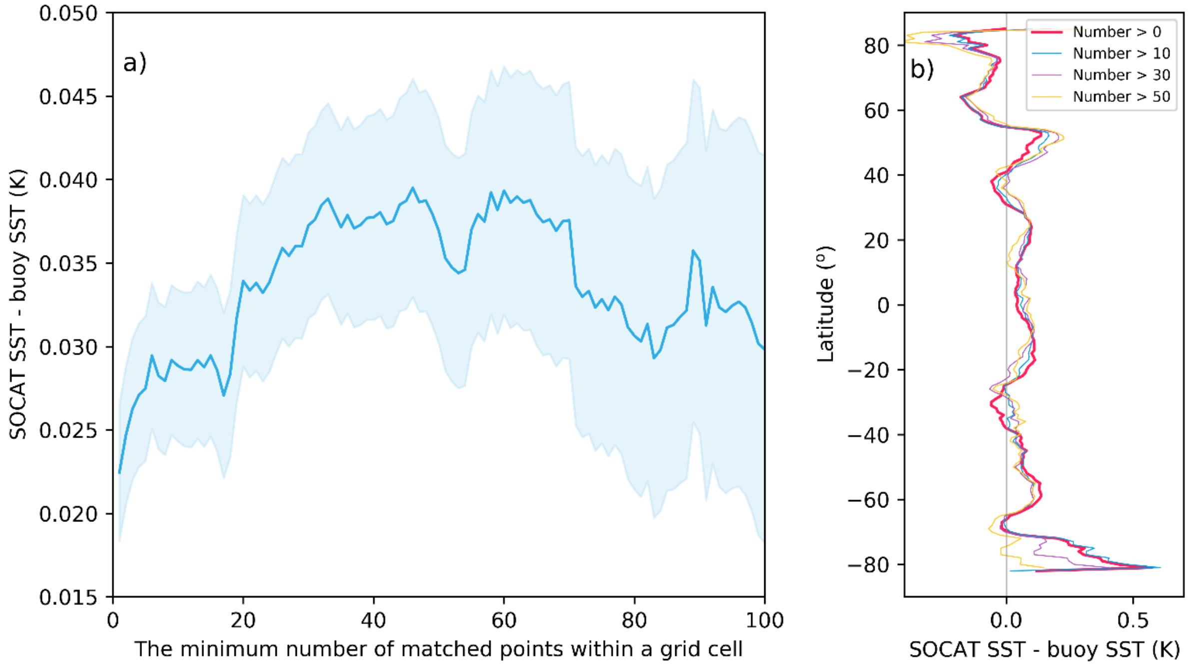

Figure. S2. (a) Average of SOCAT SST minus buoy SST (from 1982 to 2020) versus the minimum number of matched points within a grid cell, and (b) the latitudinal variation of SOCAT SST minus buoy SST. The first (second) point in (a) represents the average temperature difference considering all grid cells with at least one (two) SOCAT and one (two) buoy measurement (s). The blue shading indicates one standard deviation. The red, blue, purple, and orange lines in (b) correspond to the average temperature difference for grid cells with at least one, eleven, thirty one, and fifty one matched SOCAT and buoy measurements, respectively .

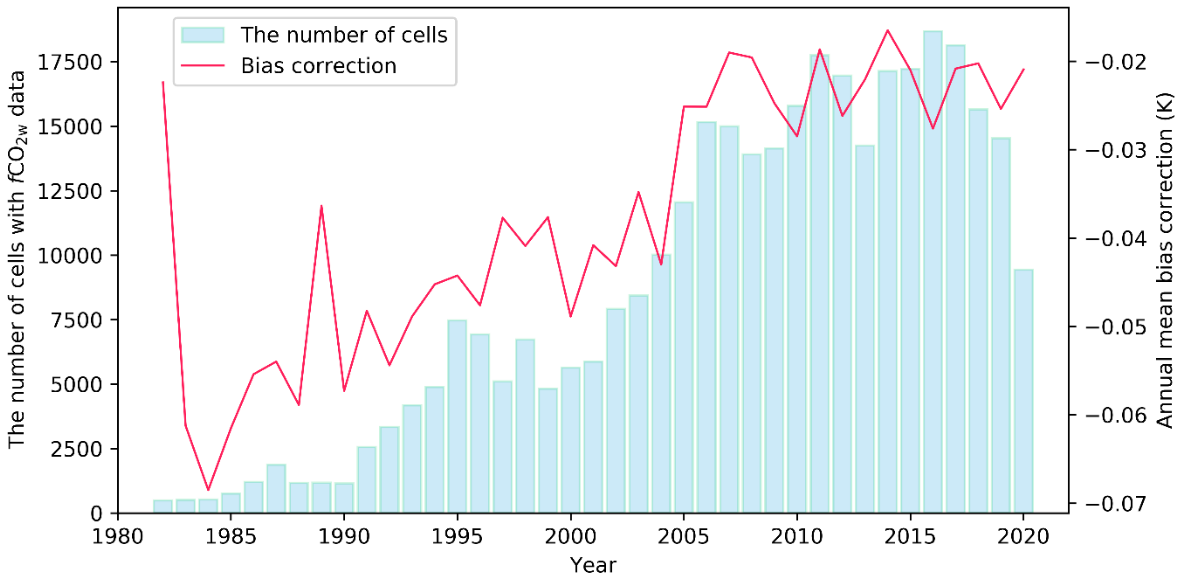

Figure S3. The number of grid cells (per year) with measurements in the 1° × 1°, monthly gridded SOCAT data (blue bars) and the inter-annual mean bias correction for the SOCAT SST (red line) assessed by the buoy SST.

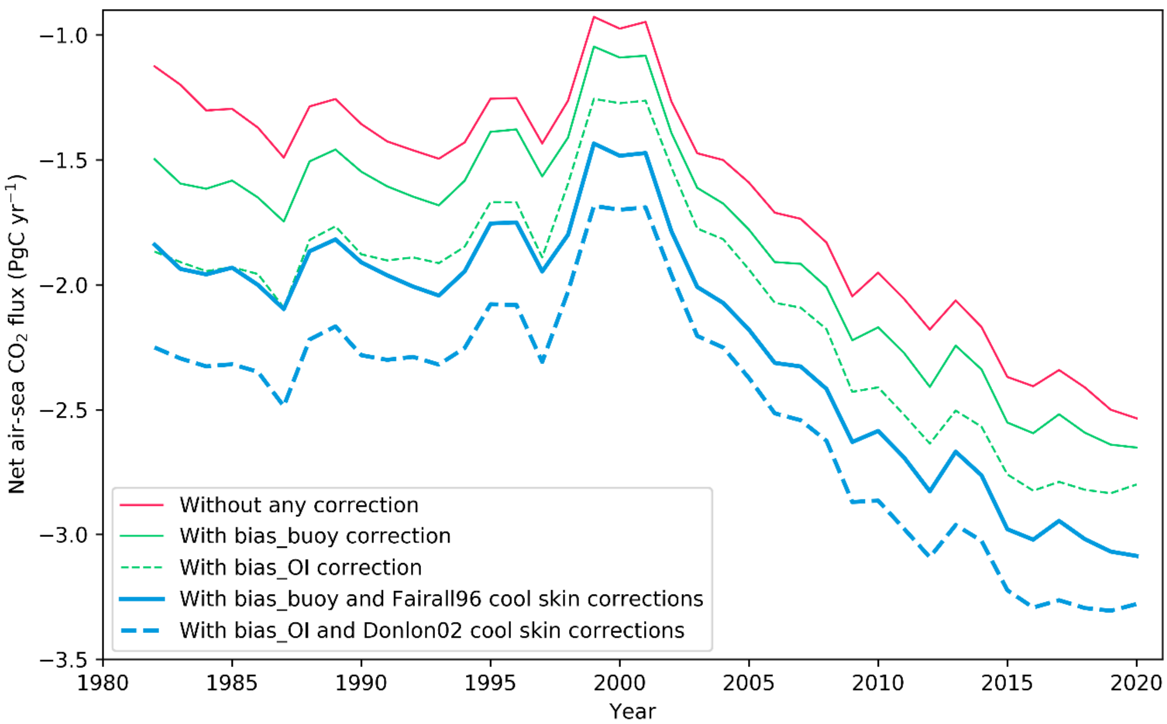

Figure S4. Time series of the annual mean global net air-sea CO_2 flux calculated by interpolating the sea surface CO_2 fugacity ($f\mathrm{CO}_{2w}$) data in SOCATv2021 using a neural network-based method (Landschützer et al., 2013). Negative values represent ocean CO_2 uptake. The red, green, and blue solid lines represent the uncorrected flux, the flux with bias_buoy correction (bias assessed by buoy SST), and the flux with bias_buoy and Fairall96 cool skin corrections, respectively (this study). The green and blue dashed curves correspond to the flux with the bias_OI (using co-located DOISST v2.1 to account for the bias in SOCAT SST) and Donlon02 cool skin corrections (Watson et al., 2020). The same datasets, interpolation method (Landschützer et al., 2013), and the Arctic and the coastal flux compensation method (Fay et al., 2021) are used for the flux calculations in the figure.

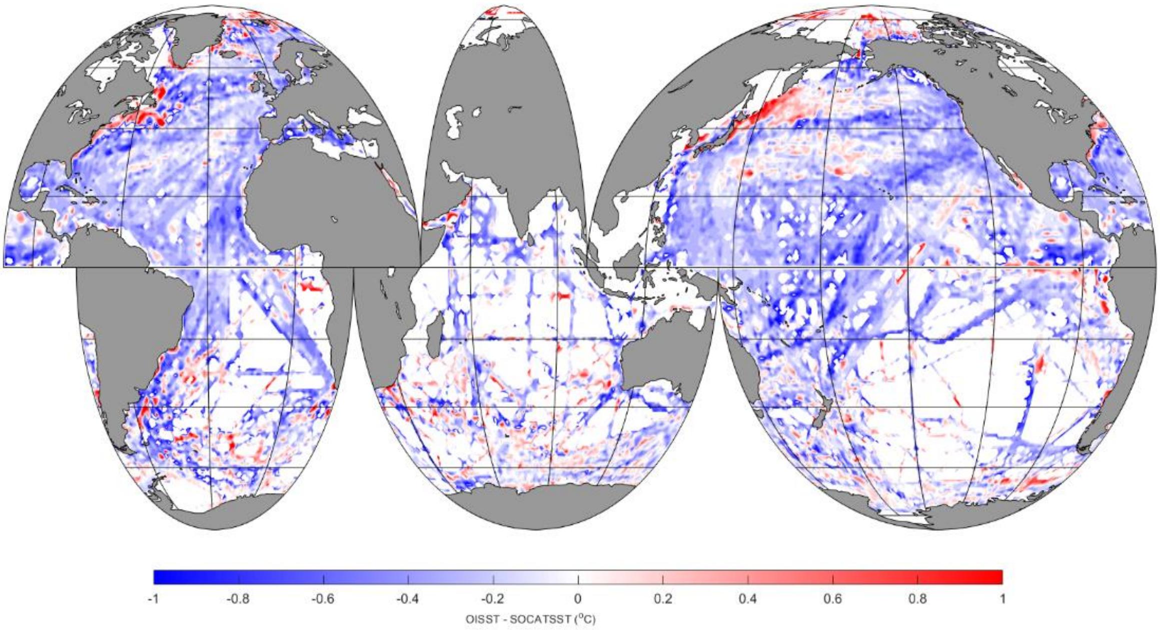

Figure S5. Mean difference between the OISST and the gridded SOCAT SST for 1982 to 2020. The positive (negative) value represents the OISST is higher (lower) than the SOCAT SST.

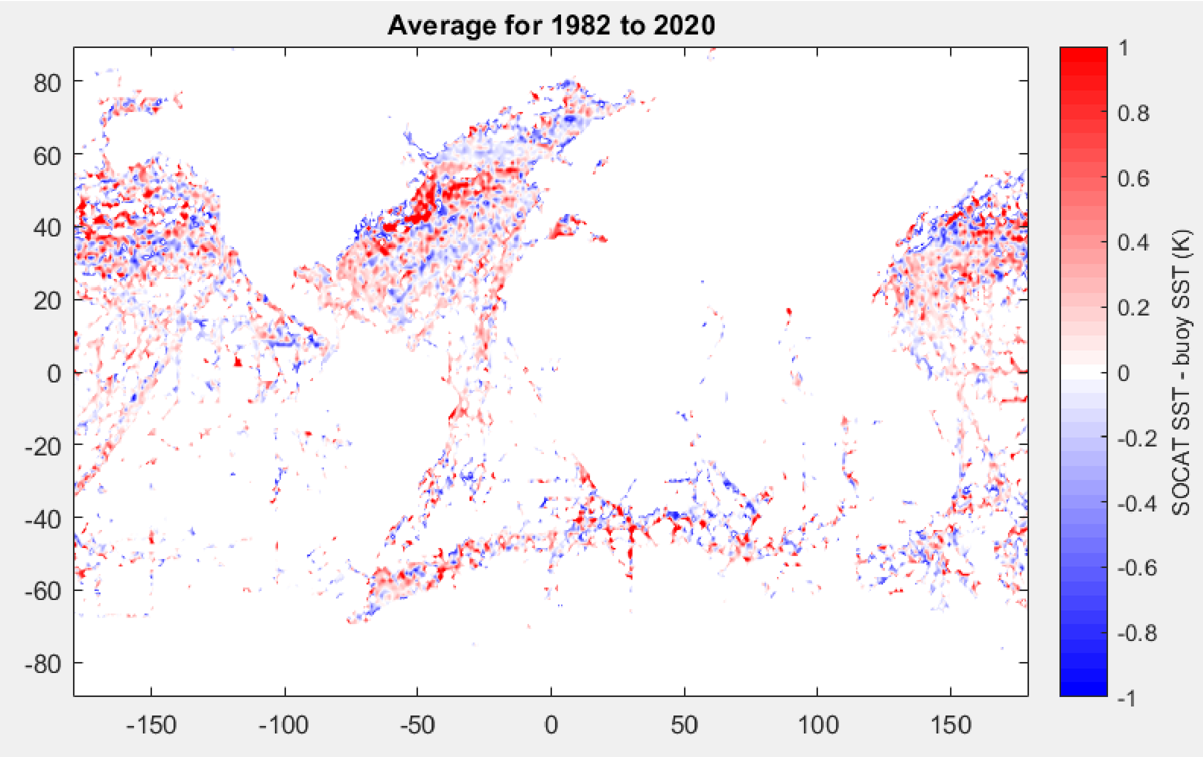

Figure S6. Mean difference between the gridded SOCAT SST and the gridded buoy SST for 1982 to 2020. The positive (negative) value represents the SOCAT is higher (lower) than the buoy SST.

Table S1. Summary of the SST datasets used in global air-sea CO_2 flux estimates by the bulk flux method (Equation 1 in the main text). Acronyms of SST products and related references are in the footnotes.

Studies	***Sc* and α_w**	**α_i and fCO_{2a}**	**Individual fCO_{2w}**	**fCO_{2w} mapping**
Takahashi et al. (2009)	ASMD	ASMD	*In-situ* T_{Bulk}	Interpolated T_{Bulk}
Rödenbeck et al. (2013)	OAFlux	OAFlux	*In-situ* T_{Bulk}	OAFlux
Zeng et al. (2014) and Landschützer et al. (2016)	MOISST v2	MOISST v2	*In-situ* T_{Bulk}	MOISST v2
Denvil-Sommer et al. (2019)	ARMOR3D	ARMOR3D	*In-situ* T_{Bulk}	ARMOR3D
Gregor et al. (2019)	DOISST v2.0	DOISST v2.0	*In-situ* T_{Bulk}	DOISST v2.0
Watson et al. (2020)	DOISST v2.0	DOISST v2.0 – 0.17 K	Co-located DOISST v2.0	HadISST
Iida et al. (2021)	MGDSST	MGDSST	*In-situ* T_{Bulk}	MGDSST
This study	CCI SST v2.1	CCI SST v2.1 with a Fairall96 cool skin correction	*In-situ* T_{Bulk} with a bias correction assessed by buoy SST	CCI SST v2.1

ASMD: surface water temperature from the NOAA Atlas of Surface Marine Data (1994, as cited in Takahashi et al., 2009). OAFlux: SST from the Objectively Analysed Air-Sea Fluxes for the global oceans dataset (Yu & Weller, 2007). MOISST v2: NOAA Monthly Optimum Interpolation SST dataset version 2, also known as OI.V2 SST (Reynolds et al., 2002). ARMOR3D: SST from monthly global reprocessed products of physical variables from the ARMOR3D L4 dataset (Guinehut et al., 2012). DOISST v2.0: NOAA Daily Optimum Interpolation SST dataset version 2 (Banzon et al., 2016; Reynolds et al., 2007). HadISST: Hadley Centre Sea Ice and Sea Surface Temperature dataset (Rayner et al., 2003). MGDSST: Merged satellite and *in-situ* data global daily SST analysis dataset (Sakurai et al., 2005). CCI SST v2.1: European Space Agency Climate Change Initiative SST product (Merchant et al., 2019; Merchant & Embury, 2020). *In-situ* T_{Bulk} represents the *in-situ* bulk SST measurements in the LDEO and SOCAT datasets. The study of Takahashi et al. (Takahashi et al., 2009) used the LDEO (Lamont-Doherty Earth Observatory) fCO_{2w} dataset (Takahashi et al., 2008) while the other studies employed the SOCAT fCO_{2w} dataset (Bakker et al., 2016). Co-located DOISST v2.0: the 0.25° × 0.25°, daily DOISST v2.0 is resampled to 1° × 1°, monthly data and then co-located with the individual fCO_{2w} measurements in SOCAT (Goddijn-Murphy et al., 2015).

Dataset S1 (Separate file: Flux corrections with different methods. xlsx): Air-sea CO_2 flux corrections using different methods. Lines 2–5 represent the flux corrections for different years using bias_buoy, bias_OI, Fairall96, and Donlon02 temperature corrections, respectively. Lines 7–10 correspond to the flux corrections for different latitude bins using bias_buoy, bias_OI, Fairall96, and Donlon02 temperature corrections, respectively. For example, latitude -89.5 represent the median latitude of the latitude bin [-90, -89] and the corresponding flux correction represent the accumulated flux in this latitude bin.

SI References

Bakker, D. C. E., Bange, H. W., Gruber, N., Johannessen, T., Upstill-Goddard, R. C., Borges, A. V, et al. (2014). Air-sea interactions of natural long-lived greenhouse gases (CO_2, N_2O, CH_4) in a changing climate. In P. S. Liss & M. T. Johnson (Eds.), *Ocean-atmosphere interactions of gases and particles* (pp. 113–169). Berlin, Heidelberg: Springer Berlin Heidelberg. https://doi.org/10.1007/978-3-642-25643-1_3

Bakker, D. C. E., Pfeil, B., Landa, C. S., Metzl, N., O'Brien, K. M., Olsen, A., et al. (2016). A multi-decade record of high-quality fCO_2 data in version 3 of the Surface Ocean CO_2 Atlas (SOCAT). *Earth System Science Data*, *8*(2), 383–413. https://doi.org/10.5194/essd-8-383-2016

Banzon, V., Smith, T. M., Mike Chin, T., Liu, C., & Hankins, W. (2016). A long-term record of blended satellite and in situ sea-surface temperature for climate monitoring, modeling and environmental studies. *Earth System Science Data*, *8*(1), 165–176. https://doi.org/10.5194/essd-8-165-2016

Denvil-Sommer, A., Gehlen, M., Vrac, M., & Mejia, C. (2019). LSCE-FFNN-v1: a two-step neural network model for the reconstruction of surface ocean pCO_2 over the global ocean. *Geoscientific Model Development*, *12*(5), 2091–2105. https://doi.org/10.5194/gmd-12-2091-2019

Fay, A. R., Gregor, L., Landschützer, P., McKinley, G. A., Gruber, N., Gehlen, M., et al. (2021).

SeaFlux: Harmonization of air-sea CO_2 fluxes from surface pCO_2 data products using a standardized approach. *Earth System Science Data*, *13*(10), 4693–4710. https://doi.org/10.5194/essd-13-4693-2021

Freeman, E., Woodruff, S. D., Worley, S. J., Lubker, S. J., Kent, E. C., Angel, W. E., et al. (2017). ICOADS Release 3.0: a major update to the historical marine climate record. *International Journal of Climatology*, *37*(5), 2211–2232. https://doi.org/10.1002/joc.4775

Goddijn-Murphy, L. M., Woolf, D. K., Land, P. E., Shutler, J. D., & Donlon, C. (2015). The OceanFlux Greenhouse Gases methodology for deriving a sea surface climatology of CO_2 fugacity in support of air-sea gas flux studies. *Ocean Science*, *11*(4), 519–541. https://doi.org/10.5194/os-11-519-2015

Gregor, L., Lebehot, A. D., Kok, S., & Scheel Monteiro, P. M. (2019). A comparative assessment of the uncertainties of global surface ocean CO_2 estimates using a machine-learning ensemble (CSIR-ML6 version 2019a)-Have we hit the wall? *Geoscientific Model Development*, *12*(12), 5113–5136. https://doi.org/10.5194/gmd-12-5113-2019

Guinehut, S., Dhomps, A. L., Larnicol, G., & Le Traon, P. Y. (2012). High resolution 3-D temperature and salinity fields derived from in situ and satellite observations. *Ocean Science*, *8*(5), 845–857. https://doi.org/10.5194/os-8-845-2012

Huang, B., Thorne, P. W., Banzon, V. F., Boyer, T., Chepurin, G., Lawrimore, J. H., et al. (2017). Extended reconstructed sea surface temperature, version 5 (ERSSTv5): Upgrades, validations, and intercomparisons. *Journal of Climate*, *30*(20), 8179–8205. https://doi.org/10.1175/JCLI-D-16-0836.1

Huang, B., Liu, C., Banzon, V., Freeman, E., Graham, G., Hankins, B., et al. (2021). Improvements of the daily optimum interpolation sea surface temperature (DOISST) version 2.1. *Journal of Climate*, *34*(8), 2923–2939. https://doi.org/10.1175/JCLI-D-20-0166.1

Iida, Y., Takatani, Y., Kojima, A., & Ishii, M. (2021). Global trends of ocean CO_2 sink and ocean acidification: an observation-based reconstruction of surface ocean inorganic carbon variables. *Journal of Oceanography*, *77*(2), 323–358. https://doi.org/10.1007/s10872-020-00571-5

Jähne, B. (2009). Air-sea gas exchange. *Elements of Physical Oceanography: A Derivative of the*

Encyclopedia of Ocean Sciences, 160–169. https://doi.org/10.1016/B978-0-12-409548-9.11613-6

Johnson, K. S. (1982). Carbon dioxide hydration and dehydration kinetics in seawater. *Limnology and Oceanography*, *27*(5), 849–855. https://doi.org/10.4319/lo.1982.27.5.0849

Kennedy, J. J., Rayner, N. A., Smith, R. O., Parker, D. E., & Saunby, M. (2011). Reassessing biases and other uncertainties in sea surface temperature observations measured in situ since 1850: 2. Biases and homogenization. *Journal of Geophysical Research*, *116*(D14), 1–22. https://doi.org/10.1029/2010jd015220

Kennedy, J. J., Rayner, N. A., Atkinson, C. P., & Killick, R. E. (2019). An ensemble data set of sea surface temperature change from 1850: The Met Office Hadley Centre HadSST.4.0.0.0 data set. *Journal of Geophysical Research: Atmospheres*, *124*(14), 7719–7763. https://doi.org/10.1029/2018JD029867

Landschützer, P., Gruber, N., Bakker, D. C. E., Schuster, U., Nakaoka, S., Payne, M. R., et al. (2013). A neural network-based estimate of the seasonal to inter-annual variability of the Atlantic Ocean carbon sink. *Biogeosciences*, *10*(11), 7793–7815. https://doi.org/10.5194/bg-10-7793-2013

Landschützer, P., Gruber, N., & Bakker, D. C. E. (2016). Decadal variations and trends of the global ocean carbon sink. *Global Biogeochemical Cycles*, *30*(10), 1396–1417. https://doi.org/10.1002/2015GB005359

Merchant, C. J., & Embury, O. (2020). Adjusting for desert-dust-related biases in a climate data record of sea surface temperature. *Remote Sensing*, *12*(16), 1–15. https://doi.org/10.3390/RS12162554

Merchant, C. J., Embury, O., Bulgin, C. E., Block, T., Corlett, G. K., Fiedler, E., et al. (2019). Satellite-based time-series of sea-surface temperature since 1981 for climate applications. *Scientific Data*, *6*(1), 1–18. https://doi.org/10.1038/s41597-019-0236-x

Pierrot, D., Neill, C., Sullivan, K., Castle, R., Wanninkhof, R., Lüger, H., et al. (2009). Recommendations for autonomous underway pCO_2 measuring systems and data-reduction routines. *Deep-Sea Research Part II: Topical Studies in Oceanography*, *56*(8–10), 512–522. https://doi.org/10.1016/j.dsr2.2008.12.005

Rayner, N. A., Parker, D. E., Horton, E. B., Folland, C. K., Alexander, L. V., Rowell, D. P., et al. (2003). Global analyses of sea surface temperature, sea ice, and night marine air temperature since the late nineteenth century. *Journal of Geophysical Research: Atmospheres*, *108*(14). https://doi.org/10.1029/2002jd002670

Reynolds, R. W., & Chelton, D. B. (2010). Comparisons of daily Sea surface temperature analyses for 2007-08. *Journal of Climate*, *23*(13), 3545–3562. https://doi.org/10.1175/2010JCLI3294.1

Reynolds, R. W., Rayner, N. A., Smith, T. M., Stokes, D. C., & Wang, W. (2002). An improved in situ and satellite SST analysis for climate. *Journal of Climate*, *15*(13), 1609–1625. https://doi.org/10.1175/1520-0442(2002)015<1609:AIISAS>2.0.CO;2

Reynolds, R. W., Smith, T. M., Liu, C., Chelton, D. B., Casey, K. S., & Schlax, M. G. (2007). Daily high-resolution-blended analyses for sea surface temperature. *Journal of Climate*, *20*(22), 5473–5496. https://doi.org/10.1175/2007JCLI1824.1

Rödenbeck, C., Keeling, R. F., Bakker, D. C. E., Metzl, N., Olsen, A., Sabine, C., & Heimann, M. (2013). Global surface-ocean pCO_2 and sea-Air CO_2 flux variability from an observation-driven ocean mixed-layer scheme. *Ocean Science*, *9*(2), 193–216. https://doi.org/10.5194/os-9-193-2013

Sakurai, T., Yukio, K., & Kuragano, T. (2005). Merged satellite and in-situ data global daily SST. In *Proceedings. 2005 IEEE International Geoscience and Remote Sensing Symposium, 2005. IGARSS'05.* (Vol. 4, pp. 2606–2608). IEEE.

Takahashi, T., Sutherland, S. C., & Kozyr, A. (2008). Global ocean surface water partial pressure of CO_2 database: Measurements performed during 1968-2006 (Version 1.0). *ORNL/CDIAC-152, NDP-088. Carbon Dioxide Information Analysis Center, Oak Ridge National Laboratory, US Department of Energy, Oak Ridge, TN*, *37831*, 20.

Takahashi, T., Sutherland, S. C., Wanninkhof, R., Sweeney, C., Feely, R. A., Chipman, D. W., et al. (2009). Climatological mean and decadal change in surface ocean pCO_2, and net sea-air CO_2 flux over the global oceans. *Deep Sea Research Part II: Topical Studies in Oceanography*, *56*(8–10), 554–577. https://doi.org/10.1016/J.DSR2.2008.12.009

Watson, A. J., Schuster, U., Shutler, J. D., Holding, T., Ashton, I. G. C., Landschützer, P., et al.

(2020). Revised estimates of ocean-atmosphere CO_2 flux are consistent with ocean carbon inventory. *Nature Communications*, *11*(1), 1–6. https://doi.org/10.1038/s41467-020-18203-3

Weiss, R. F. (1974). Carbon dioxide in water and seawater: the solubility of a non-ideal gas. *Marine Chemistry*, *2*(3), 203–215. https://doi.org/10.1016/0304-4203(74)90015-2

Xu, F., & Ignatov, A. (2014). In situ SST quality monitor (i Quam). *Journal of Atmospheric and Oceanic Technology*, *31*(1), 164–180. https://doi.org/10.1175/JTECH-D-13-00121.1

Yang, C., Leonelli, F. E., Marullo, S., Artale, V., Beggs, H., Nardelli, B. B., et al. (2021). Sea surface temperature intercomparison in the framework of the copernicus climate change service (C3S). *Journal of Climate*, *34*(13), 5257–5283. https://doi.org/10.1175/JCLI-D-20-0793.1

Yu, L., & Weller, R. A. (2007). Objectively analyzed air–sea heat fluxes for the global ice-free oceans (1981–2005). *Bulletin of the American Meteorological Society*, *88*(4), 527–540. https://doi.org/10.1175/BAMS-88-4-527

Zeebe, R. E., & Wolf-Gladrow, D. (2001). *CO_2 in seawater: equilibrium, kinetics, isotopes*. Elsevier Science, pp. 85–140.

Zeng, J., Nojiri, Y., Landschützer, P., Telszewski, M., & Nakaoka, S. (2014). A global surface ocean fCO_2 climatology based on a feed-forward neural network. *Journal of Atmospheric and Oceanic Technology*, *31*(8), 1838–1849. https://doi.org/10.1175/JTECH-D-13-00137.1